Bioconvection peristaltic flow of nano Eyring–Powell fluid containing gyrotactic microorganism

Asha Shivappa Kotnurkar[1] · Sunitha Giddaiah[1]

Abstract

The present paper deals with the behavior of gyrotactic microorganisms in nanofluid affected by the magnetic field and porous medium. The advantage of adding motile microorganism is to stabilize the nanoparticle suspension generated by the combined effects of buoyancy force and magnetic field. Gyrotactic microorganisms enhanced the heat transfer, mass transfer and improve the stability of the nanofluids. The mathematical model includes the equations of conservation of mass, momentum, energy, nanoparticle concentration and microorganism equations. The governing equations have been fabricated for long wavelength and low Reynolds number approximations. The solutions have been evaluated for pressure gradient, nanoparticle concentration, temperature and motile microorganism equations are solved by using a powerful technique known as the homotopy analysis method. Effects of physical parameters like a fluid parameter, Brownian motion parameter, thermophoresis parameter, bioconvection Peclet number, Hartmann number and Grashof number are considered. Obtained results are displayed in graphs. The results reveal that bioconvection decreases the pressure gradient because convection instability takes place within the system that causes convection pattern which decreases the pressure gradient. Such result helps in biomedical sciences and engineering. Since, microorganisms are favorable in the decomposition of organic material, producing oxygen and maintaining human health.

1 Introduction

Peristalsis is a form of fluid flow mechanism produced by a continuous wave of clasping and compressing the fluid flow over a channel or tube, such a mechanism is found in the swallowing of food through the oesophagus, movement of chime in gastrointestinal tracts and the vasomotion of small blood vessels in a human body. The concept of the peristaltic mechanism was first initiated by Latham [1] in 1966. After the work of Latham, Jaffrin et al. [2] in 1971 explore the peristaltic pumping system. He studied that the peristaltic flow for the long wavelength and low Reynolds number. Many researchers and scientists diverted their research interest towards the study of peristaltic transport by considering viscous and non-viscous fluids with different models and with different geometries, few references are given in the reference list [3–7]. Recent developments on the theoretical and experimental mechanism of peristaltic flow are given in the references [8–10].

The word "nanofluid" was first formulated by Choi [11]. Nanofluid is a liquid containing nanoparticles [12]. In biomedical, magnetite nanoparticles are targeted for magnetic resonance imaging (MRI) and during drug delivery. In present days, non-Newtonian fluids have received much awareness due to its applications in medical, industries and technology. To study the non-Newtonian fluids several models have been developed. Among them, the

✉ Sunitha Giddaiah, sunithag643@gmail.com; Asha Shivappa Kotnurkar, as.kotnur2008@gmail.com | [1]Department of Studies and Research in Mathematics, Karnatak University, Dharwad 580003, India.

Eyring–Powell model has certain advantages over other fluid models. Because firstly, this model holds the kinetic theory of liquid used to obtain the concentrate of the fluid model. Secondly, at low and high shear rates the concentrated model helps to recover the error-free results of viscous nanofluid. Eyring–Powell fluid model was first initiated by Eyring and Powell [13]. Many researchers are studied the peristaltic flow in different geometrics by considering the Eyring–Powell fluid model as cited in references [14–16].

The bioconvection is flow induced by collective swimming of motile microorganisms which are little denser than water [17]. The self- propelled motile microorganisms intensify the base fluid density in a particular direction. The collection of microorganisms in the upper layer makes suspension too dense that causes instability. Under such circumference, convection instability and generation of convection patterns take place. Such a quick and random movement pattern of microorganisms causes bioconvection within the system. Bioconvection instability is developed from an initial uniform suspension without an unstable density disturbance that was studied by Pedley et al. [18]. Many researchers working on the bioconvection with different geometries are given in the references [19–21]. In biological fluid mechanics, recent significant growing areas are flows including nano-bioconvection suspended with nanoparticles and base fluids. The nanoparticles are not self-propelled like motile micro-organisms, nanoparticles motion is due to thermophoresis and Brownian motion. If the concentration of nanoparticle is small, bioconvection occurs in a nanofluid. The recent developments of nano-bioconvection containing microorganisms are mentioned in references [22–26].

The porous medium is the ratio of pore volume to the total volume of a given sample of material. A porous medium is a material containing Pores. The pores typically filled with liquids. Important applications of porous medium are human lungs, kidney, vascular beds, bones and also other human health issues. The effect of the magnetic field on the peristaltic flow through porous media has been the center of attraction because of its contribution to controlling the thickness of the fluid viscosity. Peristaltic flow in presence of magnetic field and porous media is discussed in the references [27–29] and Peristaltic blood flow is discussed in the references [30, 31].

Literature review revealed that no work has been done on bioconvection peristaltic flow considering Eyring–Powell nanofluid in presence of magnetic field and porous medium. However, recently Noreen [32] has studied the bioconvection peristaltic flow containing gyrotactic microorganisms in a symmetric channel. Bhatti et al. [33] has investigated the peristaltic flow of non- Newtonian Jeffrey nanofluid in presence of coagulation and variable magnetic field containing gyrotactic microorganism in annulus. Since, Peristalsis is well known mechanism to transport the physiological fluid in most biological organs. Many biological systems are observed to be non-uniform, we purpose the study of free convection peristaltic transport in a non-uniform channel filled by Eyring–Powell nanofluid containing gyrotactic microorganism. The present study has wide range of applications in biomedical science and engineering. Since microorganisms are favorable in decomposition of organic material, producing oxygen and maintaining human health. The dilution of microorganisms in the nanofluids modifies the thermal conductivity. In the present paper, the solution for Pressure gradient, temperature, concentration and motile microorganism density along with boundary conditions are solved by using the homotopy analysis method [34, 35]. Different physical parameters on pressure gradient, temperature, nanoparticle concentration and motile-microorganisms density are analyzed through graphs.

2 Flow formulation of the problem

Consider a peristaltic flow formulation of the problem in a two-dimensional channel. The physical model of the wall surface can be written as

$$h'(\tilde{X}, \tilde{t}) = b(\tilde{X}) + d\sin\left(\frac{2\pi}{\lambda}(\tilde{X} - c\tilde{t})\right), \tag{1}$$

here $b(\tilde{X}) = a_{20} + k\tilde{X}$ is the half width of tube. Let $\tilde{U}$ and $\tilde{V}$ are velocity components. The velocity field V can be written as

$$V = (\tilde{U}, \tilde{V}, 0). \tag{2}$$

Eyring–Powell fluid model of shear stress tensor $\tilde{S}$ is

$$\tilde{S} = \mu\nabla\tilde{V} + \frac{1}{\beta}\sinh^{-1}\left(\frac{1}{c^*}\nabla\tilde{V}\right), \tag{3}$$

where μ is coefficient of shear viscosity, β and c^* are the fluid parameters.

$$\sinh^{-1}\left(\frac{1}{c^*}\nabla\tilde{V}\right) \approx \frac{1}{c^*} - \frac{1}{6}\left(\frac{1}{c^*}\nabla\tilde{V}\right)^3, \left|\frac{1}{c^*}\nabla\tilde{V}\right| <= 1. \tag{4}$$

The governing equations of mass, momentum, energy, nanoparticle mass transfer and density of motile microorganism for conservation nano Eyring–Powell fluid can be formulated as follows

$$\frac{\partial\tilde{U}}{\partial\tilde{X}} + \frac{\partial\tilde{V}}{\partial\tilde{Y}} = 0. \tag{5}$$

$$\rho_f\left(\frac{\partial \tilde{U}}{\partial \tilde{t}} + \tilde{U}\frac{\partial \tilde{U}}{\partial \tilde{X}} + \tilde{V}\frac{\partial \tilde{U}}{\partial \tilde{Y}}\right) = -\frac{\partial \tilde{p}}{\partial \tilde{X}} + \left(\mu + \frac{1}{\beta c^*}\right)\left(\frac{\partial^2 \tilde{U}}{\partial \tilde{X}^2} + \frac{\partial^2 \tilde{U}}{\partial \tilde{Y}^2}\right) - \frac{1}{2\beta c^{*3}}\left(\frac{\partial \tilde{U}}{\partial \tilde{X}} + \frac{\partial \tilde{U}}{\partial \tilde{Y}}\right)^2\left(\frac{\partial^2 \tilde{U}}{\partial \tilde{X}^2} + \frac{\partial^2 \tilde{U}}{\partial \tilde{Y}^2}\right) - \sigma B_0^2 \tilde{U}$$
$$- \frac{\mu}{k_1}\tilde{U} + (1 - \phi_1)\rho_f g\beta_1(\tilde{T} - \tilde{T}_0) - (\rho_p - \rho_f)g(\tilde{C} - \tilde{C}_0) - (\rho_m - \rho_f)\gamma g(\tilde{n} - \tilde{n}_0),$$

(6)

$$\rho_f\left(\frac{\partial \tilde{V}}{\partial \tilde{t}} + \tilde{U}\frac{\partial \tilde{V}}{\partial \tilde{X}} + \tilde{V}\frac{\partial \tilde{V}}{\partial \tilde{Y}}\right) = -\frac{\partial \tilde{p}}{\partial \tilde{Y}} + \left(\mu + \frac{1}{\beta c^*}\right)\left(\frac{\partial^2 \tilde{V}}{\partial \tilde{X}^2} + \frac{\partial^2 \tilde{V}}{\partial \tilde{Y}^2}\right) - \frac{1}{2\beta c^{*3}}\left(\frac{\partial \tilde{V}}{\partial \tilde{X}} + \frac{\partial \tilde{V}}{\partial \tilde{Y}}\right)^2\left(\frac{\partial^2 \tilde{V}}{\partial \tilde{X}^2} + \frac{\partial^2 \tilde{V}}{\partial \tilde{Y}^2}\right),$$

(7)

$$(\rho c)_f\left(\frac{\partial \tilde{T}}{\partial \tilde{t}} + \tilde{U}\frac{\partial \tilde{T}}{\partial \tilde{X}} + \tilde{V}\frac{\partial \tilde{T}}{\partial \tilde{Y}}\right) = k^*\left(\frac{\partial^2 \tilde{T}}{\partial \tilde{X}^2} + \frac{\partial^2 \tilde{T}}{\partial \tilde{Y}^2}\right) + (\rho c)_p D_B\left(\frac{\partial \tilde{C}}{\partial \tilde{X}} + \frac{\partial \tilde{C}}{\partial \tilde{Y}}\right)\left(\frac{\partial \tilde{T}}{\partial \tilde{X}} + \frac{\partial \tilde{T}}{\partial \tilde{Y}}\right) + (\rho c)_p\frac{D_T}{T_m}\left(\frac{\partial^2 \tilde{T}}{\partial \tilde{X}^2} + \frac{\partial^2 \tilde{T}}{\partial \tilde{Y}^2}\right)^2,$$

(8)

$$\frac{\partial \tilde{C}}{\partial \tilde{t}} + \tilde{U}\frac{\partial \tilde{C}}{\partial \tilde{X}} + \tilde{V}\frac{\partial \tilde{C}}{\partial \tilde{Y}} = D_B\left(\frac{\partial^2 \tilde{C}}{\partial \tilde{X}^2} + \frac{\partial^2 \tilde{C}}{\partial \tilde{Y}^2}\right) + \frac{D_T}{T_m}\left(\frac{\partial^2 \tilde{T}}{\partial \tilde{X}^2} + \frac{\partial^2 \tilde{T}}{\partial \tilde{Y}^2}\right),$$

(9)

$$\frac{\partial \tilde{n}}{\partial \tilde{t}} + \tilde{U}\frac{\partial \tilde{n}}{\partial \tilde{X}} + \tilde{V}\frac{\partial \tilde{n}}{\partial \tilde{Y}} = D_n\frac{\partial^2 \tilde{n}}{\partial \tilde{Y}^2} - \frac{bW_C}{(\tilde{C}_1 - \tilde{C}_0)}\frac{\partial}{\partial \tilde{Y}}\left(\tilde{n}\frac{\partial \tilde{C}}{\partial \tilde{Y}}\right),$$

(10)

where ρ_p is nanoparticle mass density, ρ_f is the effective density of the fluid, $(\rho c)_f$ and $(\rho c)_p$ are the heat capacity of the fluid and effective heat capacity of the nanoparticle material, respectively k^* is thermal conductivity of the fluid, g is the acceleration due to gravity, β_1 is volume expansion coefficient, K_1 is permeability constant of the

porous medium, σ is electrically conductivity of the fluid. $\tilde{C}$ is the nanoparticle concentration, $\tilde{T}$ is the temperature of the fluid. Further, D_B and D_T are the Brownian diffusion and thermophoresis diffusion coefficients, T_m is the mean fluid temperature, b and W_C are the chemotaxis and assumed to be constants of the microorganism, ϕ_1 is the volume fraction. The laboratory frame and wave frame are introduced as

$$\tilde{x} = \tilde{X} - c\tilde{t}, \qquad\qquad \tilde{y} = \tilde{Y},$$
$$\tilde{u}(\tilde{x}, \tilde{y}) = \tilde{U} - c, \qquad\qquad \tilde{v}(\tilde{x}, \tilde{y}) = \tilde{V},$$

(11)

where $(\tilde{u}, \tilde{v})$ are velocity components in $(\tilde{x}, \tilde{y})$ coordinates. Corresponding boundary conditions are

$$\left.\begin{array}{l} \tilde{\psi} = 0, \quad \tilde{u} = \dfrac{\partial \tilde{\psi}}{\partial \tilde{y}} = 0, \quad \tilde{T} = \tilde{T}_0 \quad \tilde{C} = \tilde{C}_0 \quad \tilde{n} = \tilde{n}_0 \quad at \quad \tilde{y} = 0, \\[3mm] \tilde{\psi} = q, \quad \tilde{u} = \dfrac{\partial \tilde{\psi}}{\partial \tilde{y}} = -c, \quad \tilde{T} = \tilde{T}_1, \quad \tilde{C} = \tilde{C}_1, \quad \tilde{n} = \tilde{n}_1 \quad at \quad \tilde{y} = h' = b(\tilde{x}) + d\sin\dfrac{2\pi}{\lambda}(\tilde{x}). \end{array}\right\}$$

(12)

Introducing the following dimensionless variables

$$\left.\begin{array}{l} \psi = \dfrac{\tilde{\psi}}{cb}, \quad B = \dfrac{1}{\mu\beta c^*}, \quad A = \dfrac{Bc^2}{2b^2c^{*2}}, \quad x = \dfrac{\tilde{x}}{\lambda}, \quad y = \dfrac{\tilde{y}}{b}, \quad t = \dfrac{c\tilde{t}}{\lambda}, \quad v = \dfrac{\tilde{v}}{c}, \quad u = \dfrac{\tilde{u}}{c}, \quad \delta = \dfrac{b}{\lambda}, \quad \sigma = \dfrac{\tilde{n}_0}{\tilde{n}_1 - \tilde{n}_0}, \quad \theta = \dfrac{\tilde{T} - \tilde{T}_0}{\tilde{T}_1 - \tilde{T}_0}, \\[4mm] \chi = \dfrac{\tilde{n} - \tilde{n}_0}{\tilde{n}_1 - \tilde{n}_0}, \quad \Omega = \dfrac{\tilde{C} - \tilde{C}_0}{\tilde{C}_1 - \tilde{C}_0}, \quad Re = \dfrac{\rho_f cb}{\mu}, \quad Da = \dfrac{K_1}{b^2}, \quad Pe = \dfrac{bW_C}{D_n}, \quad \beta^* = \dfrac{k^*}{(\rho c)_f}, \quad Pr = \dfrac{v}{\beta *}, \quad F = \dfrac{q}{cb}, \quad p = \dfrac{b^2\tilde{p}}{c\lambda\mu}, \\[4mm] Gr = \dfrac{(1 - \phi_1)\rho_f g\beta_1 b^2(\tilde{T}_1 - \tilde{T}_0)}{c\mu}, \quad Nr = \dfrac{(\rho_p - \rho_f)(\tilde{C}_1 - \tilde{C}_0)}{(1 - \phi_1)\beta_1(\tilde{T}_1 - \tilde{T}_0)\rho_f}, \quad M = B_0 b\sqrt{\dfrac{\sigma}{\mu}}, \quad Rb = \dfrac{(\rho_m - \rho_f)\gamma(\tilde{n}_1 - \tilde{n}_0)}{(1 - \phi_1)\beta_1(\tilde{T}_1 - \tilde{T}_0)\rho_f}, \\[4mm] Nb = \dfrac{(\rho c)_p D_B(\tilde{C}_1 - \tilde{C}_0)}{(\rho c)_f v}, \quad Nt = \dfrac{(\rho c)_p D_T(\tilde{T}_1 - \tilde{T}_0)}{(\rho c)_f T_m v}, \quad h = \dfrac{h'}{a_{20}} = 1 + \dfrac{\lambda kx}{a_{20}} + \alpha\sin 2\pi x, \quad \alpha = \dfrac{d}{a_{20}}, \end{array}\right\}$$

(13)

where A and B are dimensionless fluid parameters, Pr is the Prandtl number, Gr is the Grashof number of the local temperature, Nr is the buoyancy ratio, Pe and Rb are the bioconvection Peclet number and bioconvection Rayleigh number respectively. Nb and Nt are the Brownian motion and thermophoresis parameters, Da is Darcy number, M is magnetic field and α is the amplitude ratio. Defining stream function ψ as $u = \frac{\partial \psi}{\partial y}$ and $v = -\delta \frac{\partial \psi}{\partial x}$.

Using non-dimensional terms (13), the basic Eqs. (1)-(12) reduces to

$$\frac{\partial p}{\partial x} = (1 + B)\frac{\partial^3 \psi}{\partial y^3} - A\left(\frac{\partial^2 \psi}{\partial y^2}\right)^2 \frac{\partial^3 \psi}{\partial y^3}$$
$$- \left(M^2 + \frac{1}{Da}\right)\frac{\partial \psi}{\partial y} + Gr(\theta - Nr\Omega - Rb\chi), \tag{14}$$

$$\frac{\partial p}{\partial y} = 0, \tag{15}$$

$$\frac{\partial^2 \theta}{\partial y^2} + Pr\,Nb\frac{\partial \theta}{\partial y}\frac{\partial \Omega}{\partial y} + Pr\,Nt\left(\frac{\partial \theta}{\partial y}\right)^2 = 0, \tag{16}$$

$$\frac{\partial^2 \Omega}{\partial y^2} + \frac{Nt}{Nb}\frac{\partial^2 \theta}{\partial y^2} = 0, \tag{17}$$

$$\frac{\partial^2 \chi}{\partial y^2} - Pe\frac{\partial \Omega}{\partial y}\frac{\partial \chi}{\partial y} - Pe\chi\frac{\partial^2 \Omega}{\partial y^2} - Pe\sigma\frac{\partial^2 \Omega}{\partial y^2} = 0. \tag{18}$$

The corresponding dimensionless boundary conditions are

$$\psi = 0, \quad \frac{\partial \psi}{\partial y} = 0, \quad \theta = 0, \quad \Omega = 0, \quad \chi = 0 \text{ at } y = 0,$$
$$\left.\psi = F, \quad \frac{\partial \psi}{\partial y} = -1, \quad \theta = 1, \quad \Omega = 1, \quad \chi = 1 \text{ at } y = h = 1 + \frac{\lambda k x}{a_{20}} + \alpha \sin 2\pi x, \right\} \tag{19}$$

F is the time mean flow rate in wave frame related to the non-dimensional, Θ in the laboratory frame as given in the following form

$$F = \int_0^h \frac{\partial \psi}{\partial y}\,dy, \quad \Theta = F + 1, \tag{20}$$

where $F = \frac{q}{cb}$ and $\Theta = \frac{Q}{cb}$.

3 HAM solution

The solutions of the nonlinear Eqs. (14–18) are evaluated by using homotopy analysis method, homotopy analysis method (HAM) is general approximation solution. The method works for the nonlinear problems that contain small and large physical parameters. The Method provides great freedom to select the initial approximations and auxiliary linear operators. By using this any complicated non-linear problems can be transformed into linear subproblems.

To find the solutions of Eqs. (14)-(18). The initial guess for the Eqs. (14)-(18) are as follows

$$\psi_0(y) = \frac{y^2(3Fh - 2Fy + h^4 - hy)}{h^3}, \tag{21}$$

$$\theta_0(y) = \frac{y}{h}, \tag{22}$$

$$\Omega_0(y) = \frac{y}{h}, \tag{23}$$

$$\chi_0(y) = \frac{y}{h}. \tag{24}$$

Furthermore, the linear operator of the problem is taken as

$$L_\psi = \frac{\partial^3}{\partial y^3}, \quad L_\theta = \frac{\partial^2}{\partial y^2}, \quad L_\Omega = \frac{\partial^2}{\partial y^2}, \quad L_\chi = \frac{\partial^2}{\partial y^2}, \tag{25}$$

which satisfies the properties

$$L_\psi\left[C_1 + C_2 y + C_3\frac{y^2}{2}\right] = 0, \quad L_\theta\left[C_4 + C_5 y\right] = 0, \quad L_\Omega\left[C_6 + C_7 y\right] = 0, \quad L_\chi\left[C_8 + C_9 y\right] = 0, \tag{26}$$

According to the methodology, the zeroth-order deformation of the problems are

$$(1 - q)L_\psi\left[\psi(y, q) - \psi_0(y, q)\right] = qH_\psi h_\psi N_\psi$$
$$\left[\psi(y, q), \theta(y, q), \Omega(y, q), \chi(y, q)\right], \tag{27}$$

$$(1 - q)L_\theta\left[\theta(y, q) - \theta_0(y, q)\right] = qH_\theta h_\theta N_\theta\left[\theta(y, q), \Omega(y, q)\right], \tag{28}$$

$$(1-q)L_\Omega\big[\Omega(y,q)-\Omega_0(y,q)\big] = qH_\Omega h_\Omega N_\Omega\big[\Omega(y,q),\,\theta(y,q)\big], \tag{29}$$

$$(1-q)L_\chi\big[\chi(y,q)-\chi_0(y,q)\big] = qH_\chi h_\chi N_\chi\big[\chi(y,q),\,\Omega(y,q)\big], \tag{30}$$

where $q \in [0,1]$ is the embedding parameter, h_ψ, h_θ, h_Ω and h_χ are the non-zero auxiliary parameters, L is an auxiliary linear operator $H_\psi, H_\theta, H_\Omega$ and H_χ are the auxiliary functions. The nonlinear operators N_ψ, N_θ, N_Ω and N_χ can be written as

$$N_\psi\big[\psi(y,q),\,\theta(y,q),\,\Omega(y,q),\,\chi(y,q)\big]$$
$$= (1+B)\frac{\partial^4\psi(y,q)}{\partial y^4} - A\frac{\partial}{\partial y}\left(\frac{\partial^2\psi(y,q)}{\partial y^2}\right)^2\frac{\partial^3\psi(y,q)}{\partial y^3}$$
$$- \left(M^2 + \frac{1}{Da}\right)\frac{\partial^2\psi}{\partial y^2} \tag{31}$$
$$+ Gr\left(\frac{\partial\theta(y,q)}{\partial y} - Nr\frac{\partial\Omega(y,q)}{\partial y} - Rb\frac{\partial\chi(y,q)}{\partial y}\right),$$

Fig. 1 $\hbar$ curves for the function of $\psi(h),\theta(h),\Omega(h)$ and $\chi(h)$ at 25th order approximations when $t = 0.1$, $x = 0.2$, $\varphi = 0.6$, $Q=0.25$, $\lambda=10$, $k=0.1$, $a_{20}=2.0$, $Nt=0.4$, $Pr=6.9$, $Nb=0.4$, $\sigma=0.5$, $Gr=1.5$, $Nr=1.5$, $Rb=1.5$, $B=2.0$, $M=0.5$, $Da=0.5$, $A=0.001$, $Pe=2.0$

$$N_\theta\big[\theta(y,q),\,\Omega(y,q)\big] = \frac{\partial^2\theta(y,q)}{\partial y^2} + Pr\,Nb\frac{\partial\theta(y,q)}{\partial y}\frac{\partial\Omega(y,q)}{\partial y} + Pr\,Nt\left(\frac{\partial\theta(y,q)}{\partial y}\right)^2, \tag{32}$$

$$N_\Omega\big[\Omega(y,q),\,\theta(y,q)\big] = \frac{\partial^2\Omega(y,q)}{\partial y^2} + \frac{Nt}{Nb}\frac{\partial^2\theta(y,q)}{\partial y^2}, \tag{33}$$

$$\Omega(y,q) = \Omega_0(y) + \sum_{m=1}^\infty \Omega_m(y)q^m, \qquad \Omega_m(y) = \frac{1}{m!}\frac{\partial^m\Omega(y,q)}{\partial q^m} \tag{38}$$

$$N_\chi\big[\chi(y,q),\,\Omega(y,q)\big] = \frac{\partial^2\chi(y,q)}{\partial y^2} - Pe\frac{\partial\Omega(y,q)}{\partial y}\frac{\partial\chi(y,q)}{\partial y} - Pe\chi\frac{\overline{\partial^2\Omega\Omega(y,q)}}{\partial y^2} - Pe\sigma\frac{\partial^2\Omega(y,q)}{\partial y^2}. \tag{34}$$

The initial approximations $\psi_0(y,q)$, $\theta_0(y,q)$, $\Omega_0(y,q)$ and $\chi_0(y,q)$ approach $\psi(y,q)$, $\theta(y,q)$, $\Omega(y,q)$ and $\chi(y,q)$ respectively, when q takes the values from 0 to 1.

Evidently

$$\chi(y,q) = \chi_0(y) + \sum_{m=1}^\infty \chi_m(y)q^m, \qquad \chi_m(y) = \frac{1}{m!}\frac{\partial^m\chi(y,q)}{\partial q^m} \tag{39}$$

$$\psi(y,0) = \psi_0(y), \quad \theta(y,0) = \theta_0(y), \quad \Omega(y,0) = \Omega_0(y), \quad \chi(y,0) = \chi_0(y)$$
$$\psi(y,1) = \psi(y), \quad \theta(y,1) = \theta(y), \quad \Omega(y,1) = \Omega(y), \quad \chi(y,1) = \chi(y) \tag{35}$$

Using Taylor's series expansion, the equation of $\theta(y,q)$, $\Omega(y,q)$, $\chi(y,q)$ with embedding parameter q, can be written

Differentiating zeroth-order deformation with n-times and setting $q = 0$, we obtain mth-order deformation equations

$$\psi(y,q) = \psi_0(y) + \sum_{m=1}^\infty \psi_m(y)q^m, \qquad \psi_m(y) = \frac{1}{m!}\frac{\partial^m\psi(y,q)}{\partial q^m} \tag{36}$$

$$L_\psi\big[\psi_m(y) - \zeta_m\psi_{m-1}(y)\big] = h_\psi R_m^\psi(y), \tag{40}$$

$$L_\theta\big[\theta_m(y) - \zeta_m\theta_{m-1}(y)\big] = h_\theta R_m^\theta(y), \tag{41}$$

$$L_\Omega\big[\Omega_m(y) - \zeta_m\Omega_{m-1}(y)\big] = h_\Omega R_m^\Omega(y), \tag{42}$$

$$\theta(y,q) = \theta_0(y) + \sum_{m=1}^\infty \theta_m(y)q^m, \qquad \theta_m(y) = \frac{1}{m!}\frac{\partial^m\theta(y,q)}{\partial q^m} \tag{37}$$
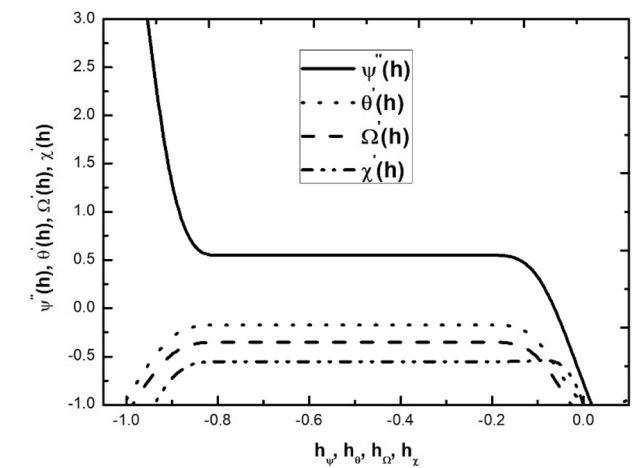
$$L_\chi\big[\chi_m(y) - \zeta_m\chi_{m-1}(y)\big] = h_\chi R_m^\chi(y). \tag{43}$$

(a)

(b)

(c)

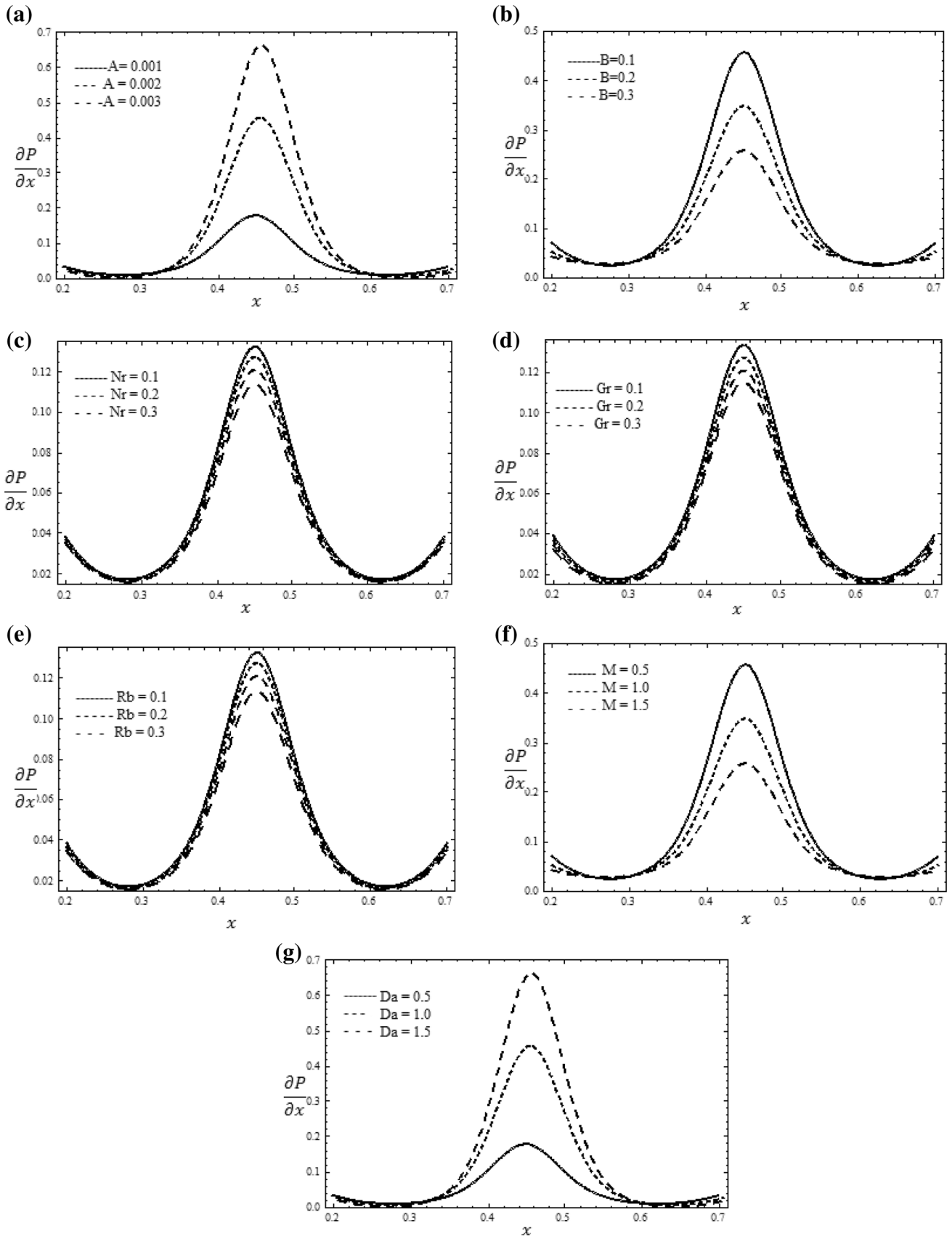
(d)

(e)

(f)

(g)

◀**Fig. 2** $\frac{dp}{dx}$ versus x, when $t = 0.1$, $x = 0.2$, $Pr = 6.9$, $\varphi = 0.6$, $Q = 0.25$, $\lambda = 10$, $k = 0.1$, $a_{20} = 2.0$, $\sigma = 0.5$, $Nt = 0.4$, $Nb = 0.4$; **a** $Gr = 1.5$, $Nr = 1.5$, $Rb = 1.5$, $B = 2.0$, $M = 0.5$, $Da = 0.5$. **b** $A = 0.001$, $Gr = 1.5$, $Nr = 1.5$, $Rb = 1.5$, $M = 0.5$, $Da = 0.5$. **c** $A = 0.001$, $B = 2.0$, $Gr = 1.5$, $Rb = 1.5$, $M = 0.5$, $Da = 0.5$. **d** $A = 0.001$, $B = 2.0$, $Nr = 1.5$, $Rb = 1.5$, $M = 0.5$, $Da = 0.5$. **e** $A = 0.001$, $B = 2.0$, $Gr = 0.4$, $Nr = 0.3$, $M = 0.5$, $Da = 0.5$. **f** $A = 0.001$, $B = 2.0$, $Gr = 0.4$, $Nr = 0.3$, $Rb = 1.5$, $Da = 0.5$. **g** $A = 0.001$, $B = 2.0$, $Gr = 0.4$, $Nr = 0.3$, $Rb = 1.5$, $M = 0.5$

where

$$R_m^\psi(y) = \frac{1}{(m-1)!} \frac{\partial^{m-1} N_\psi\left[\psi(y,q),\ \theta(y,q),\ \Omega(y,q),\ \chi(y,q)\right]}{\partial q^{m-1}}\bigg|_{q=0}, \tag{44}$$

$$R_m^\theta(y) = \frac{1}{(m-1)!} \frac{\partial^{m-1} N_\theta\left[\theta(y,q),\ \Omega(y,q)\right]}{\partial q^{m-1}}\bigg|_{q=0}, \tag{45}$$

$$R_m^\Omega(y) = \frac{1}{(m-1)!} \frac{\partial^{m-1} N_\Omega\left[\Omega(y,q),\ \theta(y,q)\right]}{\partial q^{m-1}}\bigg|_{q=0}, \tag{46}$$

$$R_m^\chi(y) = \frac{1}{(m-1)!} \frac{\partial^{m-1} N_\chi\left[\chi(y,q),\ \Omega(y,q)\right]}{\partial q^{m-1}}\bigg|_{q=0}, \tag{47}$$

$$\zeta_m = \begin{cases} 0, & m \leq 1 \\ 1, & m > 1. \end{cases} \tag{48}$$

The solutions of the problem can be easily found with the help of Mathematica.

3.1 Convergence analysis of the HAM solution

The expression $\psi(h)$, $\theta(h)$, $\Omega(h)$ and $\chi(h)$ contains the auxiliary parameters h_ψ, h_θ, h_Ω and h_χ. The auxiliary linear parameters are adjusting and controlling the homotopic solutions. Plotting the $\hbar$ curves at 25th order approximation to find the appropriate values of h_ψ, h_θ, h_Ω and h_χ (see in Fig. 1). From Fig. 1 can see that suitable values of h_ψ, h_θ, h_Ω and h_χ are $-0.8 < h_\psi < 0.2$, $-0.9 < h_\theta < -0.1$, $-0.8 < h_\Omega < 0.2$ and $-0.8 < h_\chi < 0.2$ respectively. In this problem, we choose the convergence solution $h_\psi = h_\theta = h_\Omega = h_\chi = -0.6$.

4 Discussion

In the current research paper, the results of our research problem are discussed by utilizing the homotopy analysis method with symbolic software MATHEMATICA. This section represents the detailed analysis of the various physical parameters of pressure gradient, temperature, nanoparticle concentration and density of motile microorganism profiles are analyzed.

4.1 Pressure gradient profile

Figure 2 describes the flow behavior of various physical parameters on pressure gradient. Figure 2a, b are plotted to show the behavior of fluid parameters A and B. From these two figures, one can observed that fluid parameters have opposite behavior on pressure gradient. Fluid parameter A increases with an increasing of pressure gradient, which occurs in the non-linear part of the momentum equation. The considerable part of the channel is comparatively small $x \in [0, 0.3]$ and $x \in [0.6, 0.7]$, the pressure gradient is relatively small and the flow can be easily pass without forcing of large pressure gradient. However, the tapered part of channel $x \in [0.3, 0.6]$ much immense pressure gradient is required to maintain the same flux to pass through it. Besides, the fluid parameter B increases on pressure gradient (> 0) is decreased. Since $B = \frac{1}{\mu\beta c}$, by increasing B but the viscosity of fluid μ decreases, which cause decreases in pressure gradient. Figure 2c shows the effect of buoyancy force Nr on pressure gradient. As expected, the pressure gradient decreases with increase of buoyancy parameter. This is due to the fact that buoyancy force gives rise to fluid flow. This force tends to accelerate the motion of the fluid which results in decreasing the pressure gradient. Figures 2d is plotted to show the effect of Grashof number Gr on pressure gradient. We noticed that as Grashof parameter increases and the pressure gradient is decreases. This is due to reduction in the drag force. In Fig. 2e depicted the bioconvection Rayleigh parameter effect. Convection instability takes place in the system and that cause convection pattern which decreases the pressure gradient. Figure 2f is plotted to show the effect of magnetic field M on pressure gradient. The resistance to the fluid flow by the magnetic field is represented in the Fig. 2f. It is noted that for higher values of M, pressure gradient decreases near the center of the channel. Since, Lorentz force acts like a retarding force for flow. The effect of porous medium on the pressure gradient is presented in Fig. 2g. It is noticed that the center of channel enhanced with higher values of the permeability porous medium Da.

Our results are compared with those obtained results by Rathod and Shridhar [36] in the case of no porous medium. Such as comparison is illustrated in Table 1. In this table, we have observed good agreement founded between our results and published results by Rathod and Shridhar [36] and also notice the light difference between the two

Table 1 Comparison of Pressure gradient profile for present work when $Gr=0$ $Nr=0$, $Rb=0$, $B=0$, $M=0.5$, $Da=0$ and the work obtained by Rathod and Sridhar for the values of $t=0.1$, $x=0.2$, $Q=0.25$, $\lambda=10$, $k=0.1$, $a_{20}=2.0$

φ	Rathod and Shridhar [36]	Present work
0.1	1.37132	1.37133
0.3	1.26857	1.26860
0.5	1.16462	1.16470
0.7	1.05914	1.05924
0.9	0.951852	0.95255

solutions in the middle of the channel and coincide near to the walls of the channel.

4.2 Temperature profile

Figure 3 is plotted to show the behavior of physical parameters Nb, Nt and Pr on the temperature profile θ by fixing other physical parameters. Figure 3a, b are plotted to show the behavior of temperature distribution for different values of Nb and Nt. Further, it is noticed that enhancement of temperature profile for increasing values Nt. Since, the collision between the particles enhance the fluid particles which produce plenty of heat, so it raises the temperature. Physically, thermophoresis parameter and Brownian motion parameter regulate the concentration fields due to the random motion of the particles. Brownian motion and thermophoresis parameters are showing the mixed response in temperature. Figure 3c describes the Prandtl number effect. It is observed that increases in Prandtl number Pr the temperature distribution increases. It is fact that the rising values of Prandtl number enhance the thermal field. This leads to suppress the heat transfer.

4.3 Concentration profile

The Fig. 4 describes the various physical parameters Nt, Nb and Pr on nanoparticles concentration profile. In Fig. 4a, we have observed that the nanoparticles concentration increases with an increasing Brownian motion parameter. This fact is due to huge transfer of nanoparticle from cold region to hot region which yield the increment of concentration distribution. Figure 4b shows the effect of thermophoresis parameter, when the thermophoresis parameter increased, the concentration nanoparticle decreases. The decline in nanoparticle concentration is examined due to inference in fluid molecules. Since, in thermophoresis, where the particles are moved away from the hot region to cold region, which results the disturbances in nanoparticle and hence there is a decrease in concentration of nanoparticles. The Fig. 4c describes the flow of nanoparticle
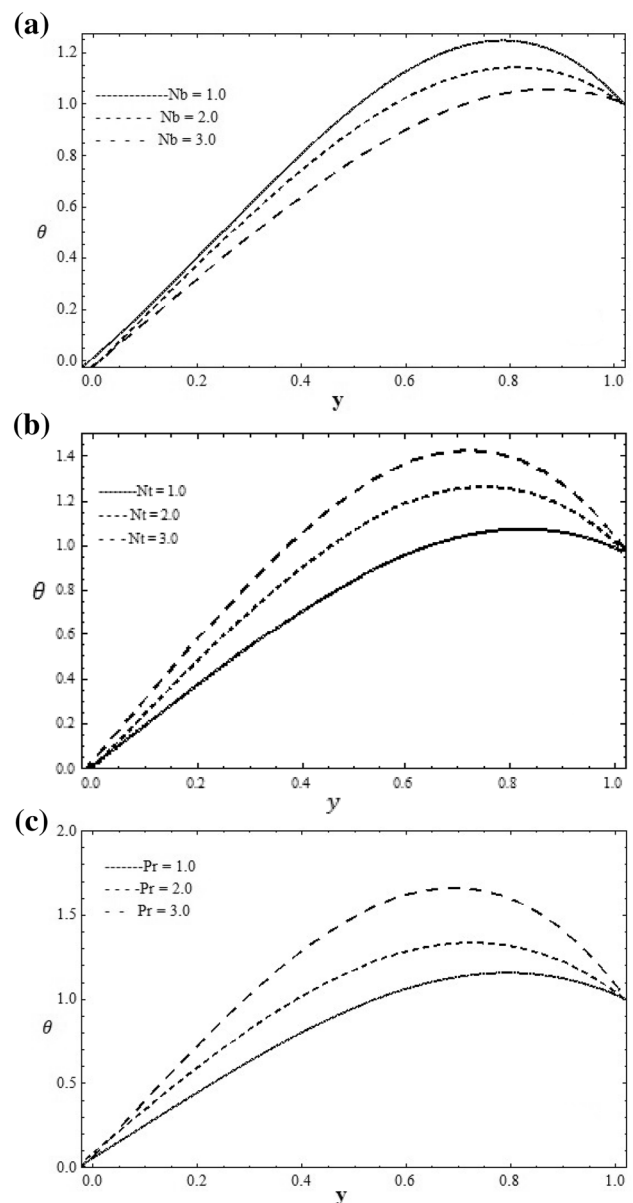
Fig. 3 Temperature θ versus y when $t=0.1$, $x=0.2$, $\varphi=0.6$, $Q=0.25$, $\lambda=10$, $k=0.1$, $a_{20}=2.0$; **a** $Nt=0.4$, $Pr=6.9$. **b** $Pr=6.9$, $Nb=0.4$. **c** $Nt=0.4$, $Nb=0.4$

concentration decreases when the Prandtl number is increased. As the Prandtl number Pr increases the thermal conductivity of the fluid decreases thus the concentration of nanoparticle decreases. Since, it is evident that the rising values of Prandtl number declines the concentration field. This leads to enhance the mass transfer.

4.4 Density of motile microorganism profile

Figure 5 describes the behavior of motile microorganism profile for different values of physical parameters. From
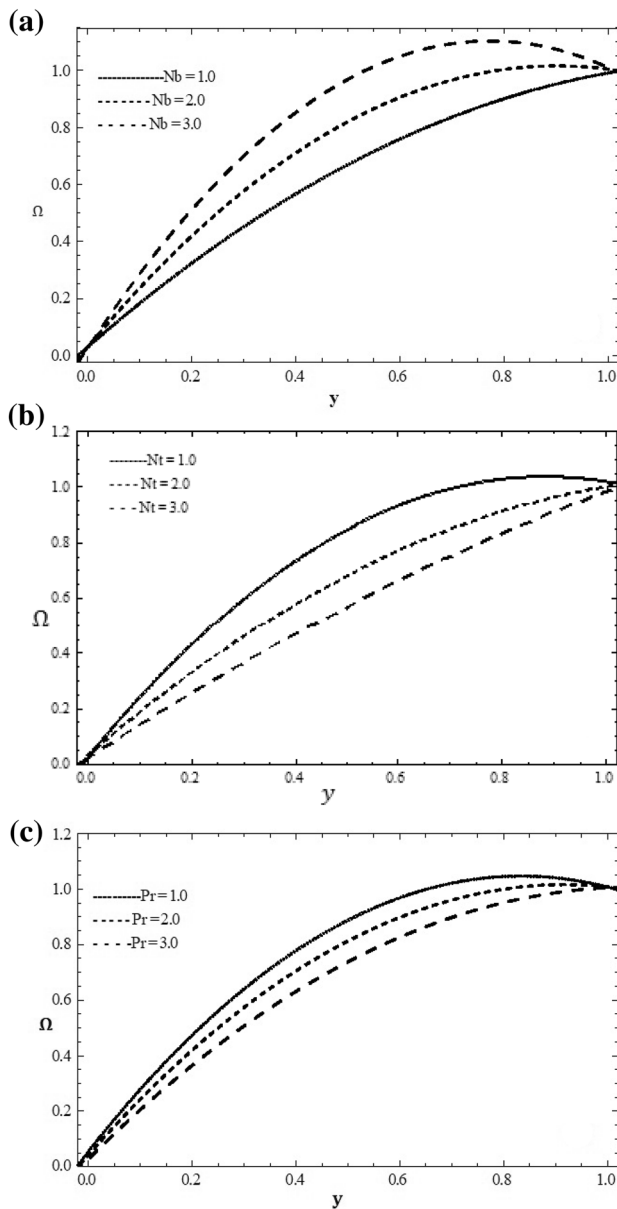
(a)

(b)

(c)

Fig. 4 Concentration Ω versus y when $t = 0.1$, $x = 0.2$, $\varphi = 0.6$, $Q = 0.25$, $\lambda = 10$, $k = 0.1$, $a_{20} = 2.0$; **a** $Nt = 0.4$, $Pr = 6.9$. **b** $Pr = 6.9$, $Nb = 0.4$. **c** $Nt = 0.4$, $Nb = 0.4$

Fig. 5a, it is observed that the density of motile microorganism profile increases with an increase of Brownian motion parameter Nb. It is obvious that motile microorganism transfer rate increases when Nb is increased. Figure 5b depicted the thermophoresis parameter effect on the motile microorganism density, it is noticed that density of motile microorganism profile decreased when the thermophoresis parameter Nt increases. Enhancement Nt

brings the nanoparticle at higher state heat region which increases the fluid temperature. Hence the density of microorganism decreases.

In Fig. 5a, b, we observed that the presence of Brownian motion and thermophoresis parameter affects the swim of microorganism. The bioconvection takes place in suspension of nanoparticles. Based on Oberbeck-Boussinesq approximation. Figure 5a shows the enhancement of the density of microorganism to swim in the upward directions and Fig. 5b shows the reduction in the density of up word swimming microorganism. Figure 5c expresses the effect of bioconvection Peclet number on motile microorganism density. It is observed that as bioconvection Peclet number increases the motile microorganism density decreases. Since, stronger Peclet number intimates weaker Brownian motion diffusion coefficients which results relatively small penetration depth for swimming of microorganism. In Fig. 5d shows the effect of bioconvection constant σ on motile microorganism density. The motile microorganism density appears to be decreases when bioconvection constant is increases. Physically, this can be traced to the fact the effects of Lorentz force on density fluid flow and consequently on shear stress are more substantial.

5 Conclusion

Here we analyzed the bioconvection peristaltic flow of a nano Eyring–Powell fluid through non-uniform channel containing gyrotactic microorganism is investigated under long wavelength and low Reynolds number approximations. The results are displayed in the form of graphs and following the important points are mentioned below.

- Pressure gradient gives opposite behavior with increasing values of Eyring–Powell fluid parameters A and B.
- The opposite behavior observed on the pressure gradient for magnetic field M and porous medium Da.
- Opposite behavior of nanoparticle concentration and temperature profiles increases with a Brownian motion parameter, thermophoresis parameter and Prandtl number.
- Pressure gradient profile decreases with increasing values of Grashof number, buoyancy ratio and bioconvection Rayleigh number.
- Density of motile microorganism gives the opposite outcomes increasing values of Brownian motion parameter and thermophoresis parameter.
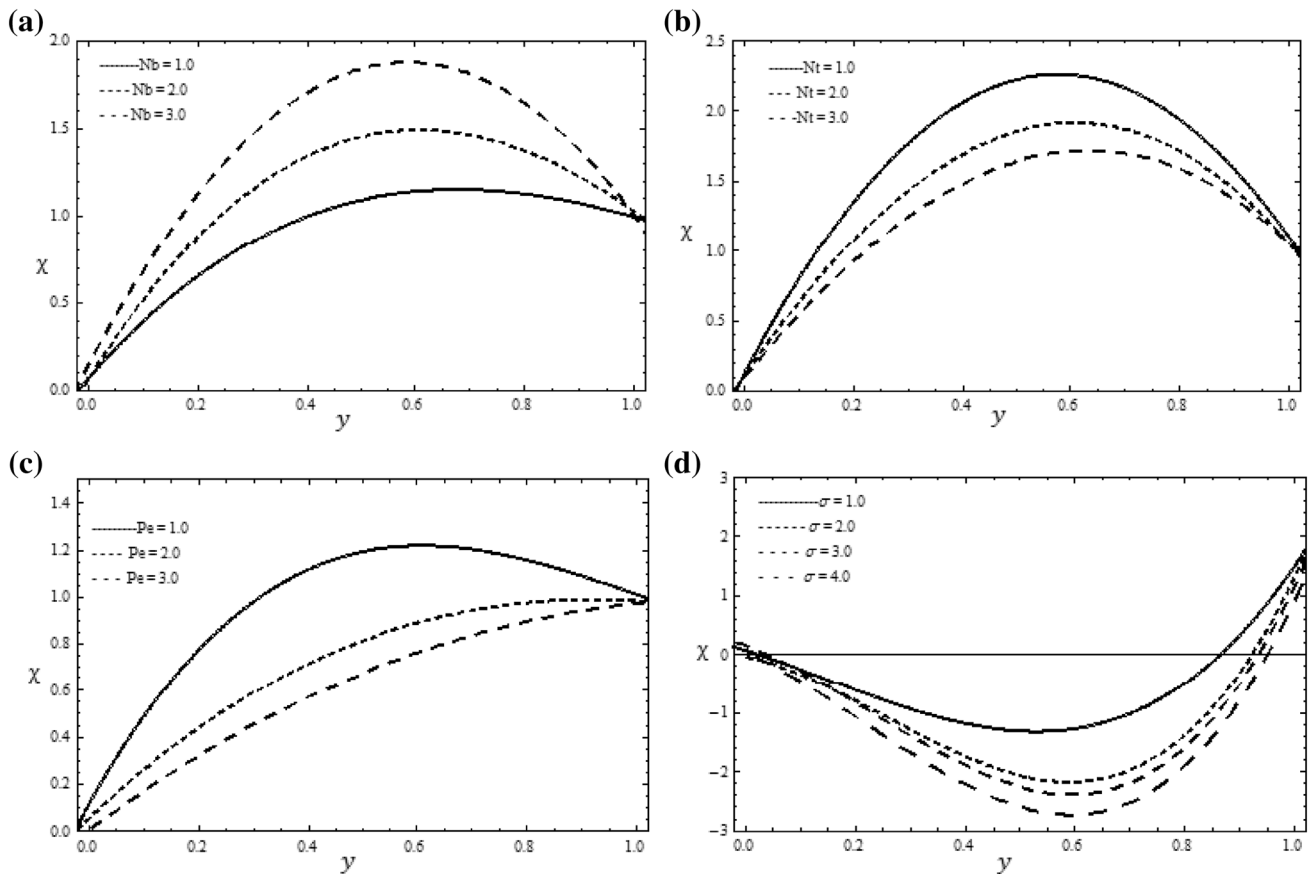
Fig. 5 Motile microorganism density versus y when $t = 0.1$, $x = 0.2$, $Pr = 6.9$, $\varphi = 0.6$, $Q = 0.25$, $\lambda = 10$, $k = 0.1$, $a_{20} = 2.0$; **a** $\sigma = 0.5$, $Nt = 0.4$, $Pe = 2.0$. **b** $\sigma = 0.5$, $Nb = 0.4$, $Pe = 2.0$. **c** $Nb = 0.4$, $\sigma = 0.5$, $Nt = 0.4$. **d** $Pe = 2.0$, $Nt = 0.4$, $Nb = 0.4$

- Similar behavior for density of motile microorganism profile increases with increasing values of bioconvection Peclet number and bioconvection constant.

References

1. Latham TW (1966) Fluid motion in a peristaltic pump. MS. Thesis. M.I.T. Cambridge
2. Jaffrin MY, Shapiro AH (1971) Peristaltic pumping. Annu Rev Fluid Mech 3:13–16. https://doi.org/10.1146/annurev.fl.03.010171.000305
3. Hayat T, Tanveer A, Yasmin H, Alsaedi A (2014) Effects of convective conditions and chemical reaction on peristaltic flow of Eyring–Powell fluid. Appl Bionics Biomech. 11(4):221–233. https://doi.org/10.3233/ABB-140100
4. Khan AA, Masood F, Ellahi BMM (2018) Mass transport on chemicalized fourth-grade propagating peristaltically through a curved channel with magnetic effects. J Mol Liq 258:186–195. https://doi.org/10.1016/j.molliq.2018.02.115
5. Nooren Sher Akbar (2014) Peristaltic sisko nanofluid in an asymmetric channel. Appl Nanosci 4(6):663–673
6. Akbar NS, Raza M, Ellahi R (2016) Impulsion of induced magnetic field for Brownian motion of nanoparticles in peristalsis. Appl Nanosci 6:359–370
7. Bhatti MM, Zeenshan A, Ellahi R (2017) Electro magnetohydrodynamic (EMHD) peristaltic flow of solid particles in a third grade fluid with heat transfer. Mech. Ind. 18(3):314–323. https://doi.org/10.1051/meca/2016061
8. Mekheimer KHS (2005) Peristaltic transport of Newtonian fluid through uniform and non-uniform annulus. Arab J Sci Eng 30:69–83
9. Asha SK, Sunitha G (2018) Mixed convection peristaltic flow of a Eyring–Powell nanofluid with magnetic field in a non-uniform channel. J Appl Math Comput 2(8):332–344
10. Asha SK, Sunita G (2017) Effect of couple stress in peristaltic transport of blood flow by homotopy analysis method. AJST 8(12):6958–6964
11. Choi SUS (1995) Enhancing thermal conductivity of fluids with nanoparticle. In: Stephen US, Eastman JA (eds) ASME

international mechanical engineering congress and exposition, San Francisco, CA, pp 12–17

12. Choi SUS (2009) Nanofluids: from vision to reality through research. J Heat Transf Trans. 131(3):033106. https://doi.org/10.1115/1.3056479

13. Powell RE, Eyring H (1994) Mechanism for the relaxation theory of viscosity. Nature 154(55):427–428

14. Abbasi FM, Alsaedi A, Hayat T (2014) Peristaltic transport of Eyring–Powell fluid in a curved channel. J Aerosp Eng. https://doi.org/10.1061/(ASCE)AS.1943-5525.0000354

15. Asha SK, Sunitha G (2018) Effect of joule heating and MHD on peristaltic blood flow of Eyring–Powell nanofluid in a non-uniform channel. JTUSCI. 13(1):155–168. https://doi.org/10.1080/16583655.2018.1549530

16. Ali H, Abdulhadi A (2017) Influence of magnetic field on peristaltic transport for Eyring–Powell fluid in a symmetric channel during a porous medium. Math Theory Model 9:9–22

17. Platt JR (1961) Bioconvection patterns in cultures of free-swimming organisms. Science 133(3466):1766–1771. https://doi.org/10.1126/science.133.3466.1766

18. Pedley TJ, Hill NA, Kessler JO (1988) The growth of bioconvection patterns in a uniform suspension of gyrotactic microorganisms. J Fluid Mech 195:223–237. https://doi.org/10.1017/S0022112088002393

19. Avramenko AA, Kuznetsov AV (2004) Stability of a suspension of gyrotactic microorganisms in superimposed fluid and porous layers. Int Commun Heat Mass Transf 31(8):1057–1066. https://doi.org/10.1016/j.icheatmasstransfer.2004.08.003

20. Kuznetsov AV (2006) The onset of thermo-bioconvection in a shallow fluid saturated porous layer heated from below in a suspension of oxytactic microorganisms. Eur J Mech B. 25:223–233. https://doi.org/10.1016/j.euromechflu.2005.06.003

21. Sampath Kumar PB, Gireesh BJ, Mahanthesh B, Chamkha AJ (2018) Thermal analysis of nanofluid flow containing gyrotactic microorganisms in bioconvection and second order slip with convective conditions. J Therm Anal Calorim. https://doi.org/10.1007/s10973-018-7860-0-

22. Kuznetsov Andrey V (2011) Nanofluid bioconvection in water-based suspensions containing nanoparticles and oxytactic microorganism: oscillatory instability. Nanoscale Res Lett 100(6):1–13. https://doi.org/10.1186/1556-276X-6-100

23. Mehryan SAM, Kashkooli FM, Soltani M, Raahemifar K (2016) Fluid flow and heat transfer analysis of a nanofluid containing motile gyrotactic micro-organisms passing a nonlinear stretching vertical sheet in the presence of a non-uniform magnetic field; numerical approach. PLOS ONE. 11(6):1–32. https://doi.org/10.1371/journal.pone.0157598

24. Anwar Beg O, Prasad VR, Vasu B (2013) Numerical study of mixed bioconvection in porous media saturated with nanofluid containing oxytactic microorganisms. J Mech Med Biol 13(4):1–25. https://doi.org/10.1142/S021951941350067X

25. Zaib A, Rashidi MM, Chamkha AJ (2018) Flow of a nanofluid containing gyrotactic microorganism over static wedge in darcy-brinkman porous medium with convective boundary condition. J Porous Media 21(10):911–928. https://doi.org/10.1615/JPorMedia.2018019967

26. Noor Saeed khan (2018) Bioconvection in second grade nanofluid flow containing nanoparticles and gyrotactic microorganisms. Braz J Phys 48(3):227–241. https://doi.org/10.1007/s13538-018-0567-7

27. Ellahi R, Hussain HF (2015) Simultaneous effects of convective of MHD and partial slip on peristaltic flow of Jeffrey fluid in a rectangular duct. J Magn Magn Mater 93:284–292

28. Reddy MG, Reddy KV, Makinde OD (2016) Hydromagnetic peristaltic motion of a reacting and radiating couple stress fluid in an inclined asymmetric channel filled with a porous medium. Alex Eng J 55:1841–1853

29. Abo-Elkhair RE, Mekheimer K, Moawad AMA (2019) Combine impacts of electrokinetic variable viscosity and partial slip on peristaltic MHD flow through a micro-channel. Iran J Sci Technol 34(1):201–212

30. Elmaboud YA, Mekheimer KS, Emam TG (2019) Numerical examination of gold nanoparticles as a drug carrier on peristaltic blood flow through physiological vessels: cancer therapy treatment. Bio Nano Sci. https://doi.org/10.1007/s12668-019-00639-7

31. Mekheimer K, Hasona WM, Abo-Elkhair RE, Zaher AZ (2018) Peristaltic blood flow with gold nanoparticles as a third grade nanofluid in catheter: application of cancer therapy. Phys Lett A 382:85–93

32. Nooren Sher Akbar (2015) Bioconvection peristaltic flow in an asymmetric channel filled by nanofluid containing gyrotactic microorganism: bio nano engineering model. Int J Numer Method Heat 25(2):214–224. https://doi.org/10.1108/HFF-07-2013-0242

33. Bhatti MM, Zeeshan A, Ellahi R (2017) simultaneous effects of coagulation and variable magnetic field on peristaltically induced motion of Jeffrey nanofluid containing gyrotactic microorganism. Microvasc Res 112:32–42

34. Gupta VG, Gupta S (2012) Application of homotopy analysis method for solving nonlinear Cauchy problem. Surv Math Appl 7:105–116

35. Hussain Q, Latif T, Alvi N, Asghar S (2018) Nonlinear radiative peristaltic flow of hydromagnetic fluid through porous medium. Results Phys 9:121–134. https://doi.org/10.1016/j.rinp.2018.02.014

36. Rathod VP, Shridhar NG (2016) effect of magnetic field on peristaltic transport of a couple stress fluid in a channel. Adv Appl Sci Res 7(1):134–144